Supplementary Information for Hierarchy of universal entanglement in 2D measurement-based quantum computation

Jacob Miller* and Akimasa Miyake†
Center for Quantum Information and Control, Department of Physics and Astronomy, University of New Mexico, Albuquerque, NM 87131, USA

In Section A we provide a more complete discussion of SPTO, including an overview of the relevant concepts from group cohomology theory. In Section B we demonstrate the precise manner in which the 2D cluster state and the Union Jack state are examples of SPTO fixed-point states originally introduced in [1]. Finally, in Sections C and D we give the full proofs of our Theorems 1 and 2.

A. Symmetry-Protected Topological Order

We give here a more complete discussion of SPTO, and in particular the possible SPTO signatures that are allowed for an arbitrary 2D state. We restrict our discussion to systems with an on-site symmetry G, and ignore SPTO arising from global symmetries, such as time reversal, spatial inversion, or lattice point group symmetries. However, we do consider the effect of lattice translational symmetries, since this symmetry is necessary for lower-dimensional portions of our SPTO signature to be well-defined. After having given this general discussion of SPTO, we state the classification of several SPTO phases in 2D and 1D which are relevant for our purposes.

The classification of SPTO phases is closely tied to group cohomology theory, so we first give a brief introduction to some of the concepts from that field. Given a symmetry group G, we can construct n-cochains ω_n, which are functions from the direct product of n copies of G to the group of complex phases, $U(1) = \{\alpha \in \mathbb{C} \,|\, \alpha\alpha^* = 1\}$. The collection of n-cochains form an abelian group $\mathcal{C}^n(G, U(1))$ under pointwise multiplication, with the product of cochains ω_n and ω'_n given by a cochain $\omega_n\omega'_n$, where $(\omega_n\omega'_n)(g_1, \ldots, g_n) = \omega_n(g_1, \ldots, g_n)\omega'_n(g_1, \ldots, g_n)$. The identity element in $\mathcal{C}^n(G, U(1))$ is the trivial n-cochain, $\omega_n^0(g_1, \ldots, g_n) = 1$. We define an operation called the coboundary operator, $d_n : \mathcal{C}^n(G, U(1)) \to \mathcal{C}^{n+1}(G, U(1))$, by

$$(d_n\omega_n)(g_1, \ldots, g_{n+1}) = \omega_n(g_2, \ldots, g_{n+1})\omega_n^{(-1)^{n+1}}(g_1, \ldots, g_n) \prod_{k=1}^{n} \omega_n^{(-1)^k}(g_1, \ldots, g_{k-1}, g_k g_{k+1}, g_{k+2}, \ldots, g_{n+1}). \quad \text{(A1)}$$

A special role is played by the n-cocycles and n-coboundaries, which form subgroups of $\mathcal{C}^n(G, U(1))$ denoted by $\mathcal{Z}^n(G, U(1))$ and $\mathcal{B}^n(G, U(1))$, respectively. An n-cochain is an n-cocycle (resp. n-coboundary) if it lies in the kernel of d_n (resp. the image of d_{n-1}). More explicitly, $\mathcal{Z}^n(G, U(1)) = \{\, \omega_n \,|\, d_n\omega_n = \omega_{n+1}^0\}$ and $\mathcal{B}^n(G, U(1)) = \{\, \omega_n \,|\, \exists\omega_{n-1}$ s.t. $d_n\omega_{n-1} = \omega_n\}$. One can show that the composite of coboundary operators d_n and d_{n+1} is trivial, in that it sends every n-cochain to the identity $(n+2)$-cochain. This implies that every n-coboundary is an n-cocycle, so that $\mathcal{B}^n(G, U(1)) \subseteq \mathcal{Z}^n(G, U(1))$.

We define the n'th cohomology group of G, $\mathcal{H}^n(G, U(1))$, to be the (abelian group) quotient of $\mathcal{Z}^n(G, U(1))$ with respect to $\mathcal{B}^n(G, U(1))$, $\mathcal{H}^n(G, U(1)) = \mathcal{Z}^n(G, U(1))/\mathcal{B}^n(G, U(1))$. Equivalently, this is the group of equivalence classes of n-cocycles, $\mathcal{H}^n(G, U(1)) = \{\, [\omega_n] \,|\, \omega_n \in \mathcal{Z}^n(G, U(1))\}$, under the equivalence relation $[\omega_n] = [\omega'_n] \Leftrightarrow \omega_n = \omega'_n\omega''_n$, where ω''_n is an arbitrary n-coboundary. For $\omega_n \in \mathcal{Z}^n(G, U(1))$, we will call $[\omega_n] \in \mathcal{H}^n(G, U(1))$ the cohomology class associated to ω_n.

The relevance of this discussion for our purposes is that SPTO phases of G-invariant many-body systems living in d-dimensional space are classified by elements of the $(d+1)$'th cohomology group. In particular, it was shown in [1] that given any two distinct cohomology classes in $\mathcal{H}^{(d+1)}(G, U(1))$, we can construct d-dimensional "fixed point" systems labeled by the cohomology classes which belong to different SPTO phases. This construction is discussed in more detail in Section B.

An important point is that systems with both on-site G symmetry and translational symmetry admit a richer classification of SPTO phases [1]. In particular, while the SPTO phase of a system without translational symmetry can be uniquely classified by a single cohomology class, with additional translational symmetry in place, the SPTO phase is classified by a full SPTO signature Ω_d, which consists of an ordered list of different cohomology classes. For systems in 2D, this signature is of the form $\Omega_2 = \langle\langle\, [\omega_3]\,;\, [\omega_2^{(x)}]\,, [\omega_2^{(y)}]\,;\, [\omega_1]\,\rangle\rangle$, with $[\omega_3] \in \mathcal{H}^3(G, U(1))$, $[\omega_2^{(x)}], [\omega_2^{(y)}] \in \mathcal{H}^2(G, U(1))$, and $[\omega_1] \in \mathcal{H}^1(G, U(1))$. We refer to these respectively as the 2D, 1D, and 0D portions of Ω_2. For SPTO systems in d physical dimensions, there will generally be $\binom{d}{k}$ components to the k-dimensional sector of the SPTO signature, corresponding to the number of independent k-dimensional surfaces in d-dimensional space. Due to our present focus on only whether or not a system possesses

* jmilla@unm.edu
† amiyake@unm.edu

SPTO, we often use an abbreviated means of writing the components of an SPTO signature, wherein a phase label is written as 0 if it corresponds to the trivial phase, and as 1 if it corresponds to any nontrivial phase.

We now introduce a few examples of concrete SPTO phases in 2D and 1D associated with various symmetry groups. Since there is always a trivial phase for every symmetry group and dimension, we will often neglect to mention these phases.

For $G = \mathbb{Z}_2$, we have no nontrivial phases in 1D, and one nontrivial phase in 2D. Our Union Jack state lives in this nontrivial 2D $\mathbb{Z}_2$ phase when its symmetry group is taken to be $\mathbb{Z}_2$.

For $G = D_2 \simeq (\mathbb{Z}_2)^2$, we have one nontrivial phase in 1D (known as the D_2 Haldane phase), and 7 nontrivial phases in 2D. D_2 is the smallest symmetry group which is capable of manifesting SPTO in 1D.

For $G = (\mathbb{Z}_2)^3$, we have 7 nontrivial phases in 1D and 127 nontrivial phases in 2D. Using a known decomposition of 2D abelian SPTO phases (those with G abelian), we can structure the 2D $(\mathbb{Z}_2)^3$ phases as $\mathcal{H}^3((\mathbb{Z}_2)^3, U(1)) \simeq (\mathbb{Z}_2)^3 \times (\mathbb{Z}_2)^3 \times \mathbb{Z}_2$ [2]. The first (resp. second) $(\mathbb{Z}_2)^3$ factor encodes the "type I" (resp. "type II") phases, those whose nontrivial SPTO arises from only one (resp., from pairs) of the $\mathbb{Z}_2$ components in $(\mathbb{Z}_2)^3$. The last $\mathbb{Z}_2$ in the decomposition of $\mathcal{H}^3((\mathbb{Z}_2)^3, U(1))$ is the unique "type III" component of the phase, which is due to a nontrivial combination of all three $\mathbb{Z}_2$ components in $(\mathbb{Z}_2)^3$. Our Union Jack state with $(\mathbb{Z}_2)^3$ symmetry belongs to the phase $(0, 0, 1)$, meaning the unique phase with trivial type I and II SPTO, and nontrivial type III SPTO.

B. The Union Jack and Cluster States as SPTO Fixed Point States

In this Section, we demonstrate how both the Union Jack and 2D cluster states are examples of the construction of [1] for constructing special RG fixed point states with nontrivial SPTO from nontrivial cocycles of a symmetry group G. We show how our Union Jack state belongs to this class of states both for $G = \mathbb{Z}_2$ and for $G = (\mathbb{Z}_2)^3$, and how the 2D cluster state belongs to this class of states.

The construction of [1] gives a means of taking d-dimensional SPTO signatures, along with a representative $(k+1)$-cocycle for each k-dimensional component of the signature, and constructing a d-dimensional state with that SPTO signature. For our purposes, we will focus on $d = 2$, for which the 2D, 1D, and/or 0D labels are allowed to be nontrivial. We will restrict first to the case of trivial lower-dimensional SPTO (the case considered almost exclusively in [1]), and later explain how these lower-dimensional labels can be made nontrivial.

To construct a 2D state from a chosen group G and 3-cocycle ω_3, we first choose a triangulated 2D lattice on which our state will live, and assign a Hilbert space H_G to every lattice vertex. H_G has dimension $|G|$, the order of G, and is spanned by an orthonormal basis labeled by the elements of G, $\{|g\rangle\}_{g\in G}$. G acts on H_G as the regular representation u_G, with $u_g |h\rangle = |gh\rangle$ for every $g, h \in G$. We first initialize every H_G in the unique invariant state $|\phi_G\rangle = (1/\sqrt{|G|}) \sum_{g\in G} |g\rangle$, which gives a symmetric global product state with trivial SPTO. We then apply to this system a collection of 3-body unitary gates, each formed from our chosen 3-cocycle, which generates the nontrivial 2D SPTO. The 3-body unitary $\hat{\omega}_3$ generated from a 3-cocycle ω_3 is diagonal in the G-basis, and has non-zero matrix elements of

$$\langle ghf | \hat{\omega}_3 | ghf \rangle = \omega_3(g, g^{-1}h, h^{-1}f). \tag{B1}$$

Our desired state is obtained by applying $\hat{\omega}_3$ or its inverse to the vertices around every triangular cell in our chosen lattice. Whether we apply $\hat{\omega}_3$ or $\hat{\omega}_3^\dagger$ to a particular triangular cell, as well as how we match up the 3 indices in Eq. (B1) with the three sites around that cell, depend on a certain ordering of lattice vertices. While the full details are given in [1], if we restrict to 3-colorable lattices we can always choose each of the three indices to be matched up with a different vertex color in a fixed manner.

Choosing $G = \mathbb{Z}_2 \simeq \{0, 1\}$, this construction outputs qubit states, with $|\phi_G\rangle = |+X\rangle$. To produce our Union Jack state, we work with the Union Jack lattice, and choose our 3-cocycle to be

$$\omega_3(g, h, f) = \begin{cases} -1, & \text{if } (g, h, f) = (1, 1, 1) \\ +1, & \text{otherwise.} \end{cases} \tag{B2}$$

Although this 3-cocycle produces a unitary $\hat{\omega}_3$ which is distinct from CCZ, the global state it produces is nonetheless the same. This can be seen from the relation $\hat{\omega}_3^{(123)} = CCZ^{(123)}CZ^{(13)}$, which allows us to show that the transversal application of $\hat{\omega}_3$ to qubits in any 3-colorable lattice with closed (nonexistent) boundary yields the same global unitary as the transversal application of CCZ. This proves that the Union Jack state is a $\mathbb{Z}_2$ SPTO fixed point state, associated with the cocycle of Eq. (B2). Because this 3-cocycle belongs to the unique nontrivial cohomology class in $\mathcal{H}^3(\mathbb{Z}_2, U(1))$, our Union Jack state consequently has nontrivial 2D SPTO.

Showing that our Union Jack state is isomorphic to a $(\mathbb{Z}_2)^3$ SPTO fixed point state is less obvious, since the lattice vertices of such states aren't associated with qubits, but rather with 8-dimensional qudits. We can get around this difficulty by first treating each of the $\mathbb{Z}_2$ factors in $(\mathbb{Z}_2)^3$ as a separate qubit system, and imagining these three factors to be stacked vertically in three layers at each lattice site. Note that this stacking is merely a convenient means of visualizing the separate qubit factors in $(\mathbb{Z}_2)^3$, while our lattice remains a genuine 2D lattice. In this case, the state we initialize each site in is $|\phi_G\rangle = |+X\rangle^{\otimes 3}$, a tensor product of one $|+X\rangle$ state on

each layer. If we write a generic element $g \in (\mathbb{Z}_2)^3$ as $g = (g_1, g_2, g_3)$, where each $g_i \in \mathbb{Z}_2$ is associated with the i'th layer, then we can choose the following 3-cocycle

$$\omega_3'(g,h,f) = \begin{cases} -1, & \text{if } (g_1, h_2, f_3) = (1,1,1) \\ +1, & \text{otherwise,} \end{cases} \tag{B3}$$

where addition is modulo 2. Using the relation Eq. (B1), we can show that $\hat{\omega}_3'$ equals a CCZ gate on the qubits indexed by g_1, h_2, and f_3, along with other terms which cancel when $\hat{\omega}_3'$ is applied globally. In other words, $\hat{\omega}_3'$ ends up having a nontrivial action only on the qubits on the first layer of the first site acted on, the second layer of the second site, and the third layer of the third site. If we apply $\hat{\omega}_3'$ transversally to all triangular cells on a 3-colorable lattice, then at each site only one of the three layers is acted on nontrivially, with the other two layers remaining unchanged. Thus, using $\hat{\omega}_3'$ to construct a $(\mathbb{Z}_2)^3$ SPTO fixed point state defined on a Union Jack lattice with n vertices yields a state which is a tensor product of our Union Jack state on n qubits, with $|+X\rangle$ on the remaining $2n$ qubits. This proves that, up to addition/removal of ancilla $|+X\rangle$ states, the Union Jack state is a $(\mathbb{Z}_2)^3$ SPTO fixed point state, associated with the cocycle of Eq. (B3). This cocycle belongs to the nontrivial $(\mathbb{Z}_2)^3$ cohomology class described at the end of Section A, which consequently specifies the nontrivial $(\mathbb{Z}_2)^3$ SPTO phase our Union Jack state belongs to.

As the 2D cluster state only possesses lower-dimensional SPTO, we must use an extended version of the previous construction to obtain the cluster state as an SPTO fixed point state. In [1] it is shown that to generate 2D fixed point states with 1D SPTO, we can use a construction almost identical to that given above, but instead of starting with a 3-cocycle ω_3 and converting it into a 3-body gate $\hat{\omega}_3$, we start with a 2-cocycle ω_2 and convert it into a 2-body gate ω_2, which has non-zero matrix elements of

$$\langle gh|\, \hat{\omega}_2\, |gh\rangle = \omega_2(g, g^{-1}h). \tag{B4}$$

$\hat{\omega}_2$ is then applied to all edges of a chosen 2D lattice, on which one copy of $|\phi_G\rangle$ has been prepared at every vertex. To generate the 2D cluster state in this manner, we can choose $G = (\mathbb{Z}_2)^2$ and use a similar decomposition of the local Hilbert space into two qubits, stacked vertically in two layers. We then utilize the 2-cocycle

$$\omega_2(g,h) = \begin{cases} -1, & \text{if } (g_1, h_2) = (1,1) \\ +1, & \text{otherwise,} \end{cases} \tag{B5}$$

where $g_i, h_i \in \mathbb{Z}_2$ is associated with the i'th component of $g, h \in (\mathbb{Z}_2)^2$. This 2-cocycle produces a 2-body unitary $\hat{\omega}_2$ which upon global application is equivalent to a CZ gate on the qubits indexed by g_1 and h_2, and an identity gate on the rest of the qubits. In close analogy to how the Union Jack state was shown above to be a $(\mathbb{Z}_2)^3$ SPTO fixed point state, we can work with the 2-colorable square lattice and show that the transversal application of $\hat{\omega}_2$ to all edges of the lattice yields a state which is a tensor product of the 2D cluster state on n qubits, with $|+X\rangle$ on the remaining n qubits. This proves that, up to addition/removal of ancilla $|+X\rangle$ states, the cluster state is a $(\mathbb{Z}_2)^2$ SPTO fixed point state.

Finally, we note that some care is required regarding the symmetry group of the 2D cluster state. The construction we just outlined outputs the cluster state as an SPTO fixed point state with $(\mathbb{Z}_2)^2$ symmetry, similar to how the 1D cluster state is most naturally seen as possessing nontrivial SPTO associated with $(\mathbb{Z}_2)^2$ symmetry. However, as seen from Eq. (C3), if we choose any particular $(\mathbb{Z}_2)^2$ subgroup of the full $(\mathbb{Z}_2)^4$ on-site symmetry, we obtain a virtual representation of our symmetry which is non-projective in at least one direction. This leads to an SPTO signature which is either $\langle\langle\, 0\,;\, 0\,,1\,;\, 0\,\rangle\rangle$ or $\langle\langle\, 0\,;\, 1\,,0\,;\, 0\,\rangle\rangle$, rather than the SPTO signature of $\langle\langle\, 0\,;\, 1\,,1\,;\, 0\,\rangle\rangle$ which appears in Theorem 1. We interpret this fact as an indicator that for states with lower-dimensional SPTO, we must take care in choosing the symmetry group we use to arrive at an SPTO signature.

C. SPTO Signature of the 2D Cluster State

We present here a full demonstration that the SPTO signature of the 2D cluster state is $\Omega_2^{(C)} = \langle\langle\, 0\,;\, 1\,,1\,;\, 0\,\rangle\rangle$, as stated in Theorem 1. To do this, we need to determine the various cohomology classes corresponding to different components of the cluster state's signature. One known way [3] of doing this is by working with a projected entangled pair state (PEPS) description of the cluster state, and examining the behavior of the representation of its on-site symmetry group $(\mathbb{Z}_2)^4$ along the boundary.

Restricting to states which live on a square lattice, a PEPS representation consists of a rank-5 tensor, $\mathcal{A} \in H_p \otimes (H_v^*)^{\otimes 4}$, where H_p and H_v are referred to as the physical and virtual Hilbert spaces, and where H^* denotes the Hilbert space dual to H. $\mathcal{A}$ can also be interpreted as a map $\mathcal{A} : H_p^* \to (H_v^*)^{\otimes 4}$. We associate one copy of $\mathcal{A}$ to each site of our lattice, with H_p corresponding to the Hilbert space of that site, and the four H_v^*'s being used to represent correlations between our site and each of the four nearest-neighbor sites. The dimension of H_v, D_v, is the bond dimension of our PEPS representation, and can be thought of as a measure of entanglement in the system. The condition for $\mathcal{A}$ to be a PEPS representation of a many-body state $|\psi\rangle$ is that the "tensor trace" of the $\mathcal{A}$'s at every site, formed by contracting every pair of adjacent H_v^*'s using maximally entangled states $|\phi_0\rangle = \sum_{i=1}^{D_v} |i,i\rangle$, yields $|\psi\rangle$. This condition is depicted in Figure 6b.

Given a PEPS representation $\mathcal{A}$ of our many-body state $|\psi\rangle$, the condition for $|\psi\rangle$ to be invariant under our on-site symmetry G, whose physical representation

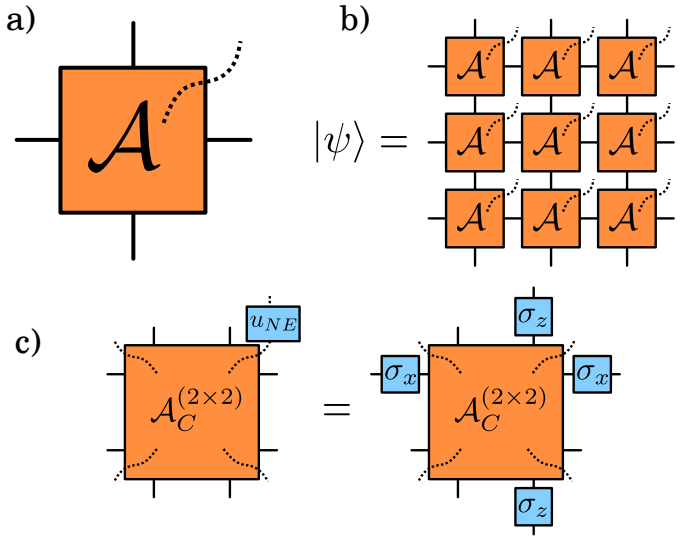

FIG. 6. a) A single PEPS tensor for a square lattice. The dotted line represents our physical system, which corresponds to a single site of our lattice, and the four solid edges represent the virtual space. b) After assigning a PEPS tensor to every site of our lattice, we obtain a physical state by taking the "tensor trace" of all tensors. This involves contracting every pair of adjacent virtual indices using a maximally entangled state $|\phi_0\rangle = \sum_{i=1}^{D_v} |i,i\rangle$, with D_v the virtual space dimension. On a lattice with no boundary, this will contract out all of the virtual spaces, leaving only our physical many-body state $|\psi\rangle$. c) An example of the physical/virtual symmetry correspondence given in Eq. (C1) for the 2D cluster state. Our PEPS tensor is defined relative to a 2×2 physical unit cell, with a four-qubit physical space and two-qubit virtual spaces. Different generators of $(\mathbb{Z}_2)^4$ will produce different combinations of X and Z on the virtual space, whose non-commutativity demonstrates the nontrivial 1D SPTO of the 2D cluster state.

is $u_G = \{\, u_g \,|\, g \in G\}$, is that there exists a virtual representation of G, $\mathcal{U}_G$, such that

$$\mathcal{A}\, u_G = e^{i\theta_G}\, \mathcal{U}_G \mathcal{A}. \tag{C1}$$

In other words, when $\mathcal{A}$ is seen as a map from the physical to the virtual space, $\mathcal{A}$ is required to be (possibly up to phase) an intertwiner between the representations u_G and $\mathcal{U}_G$. $e^{i\theta_G} = \{\, e^{i\theta_g} \,|\, g \in G\}$ is a unitary character of G, and using the fact that the collection of these characters is isomorphic to $\mathcal{H}^1(G, U(1))$, the particular choice of $e^{i\theta_G}$ ends up specifying the 0D component of our SPTO signature.

With the virtual representation $\mathcal{U}_G : (H_v^*)^{\otimes 4} \to (H_v^*)^{\otimes 4}$ in hand, we can calculate the remaining portions of the SPTO signature of our state $|\psi\rangle$. The 2D portion of this signature relates to whether or not we can decompose $\mathcal{U}_G$ into a tensor product of four unitaries on the four virtual subsystems in $(H_v^*)^{\otimes 4}$. If we cannot, such that $\mathcal{U}_G$ is necessarily an entangled representation, then our state $|\psi\rangle$ has nontrivial 2D SPTO. In such cases, there are several (somewhat involved) procedures for extracting a 3-cohomology class to classify the 2D SPTO phase, but since our current interest is in the case of trivial 2D SPTO, we won't discuss these here. The interested reader can consult [2, 4, 5] for examples of methods for obtaining information about 2D SPTO.

Given trivial 2D SPTO, we can write $\mathcal{U}_G$ as a tensor product of four terms, which we will assume has the form $\mathcal{U}_G = U_G^{(x)} \otimes (U_G^{(x)})^* \otimes U_G^{(y)} \otimes (U_G^{(y)})^*$. These four terms correspond to, in order, the left, right, top, and bottom portions of our virtual representation, where $(U_G^{(x)})^*$ (resp. $(U_G^{(y)})^*$) represent the complex-conjugated versions of $U_G^{(x)}$ (resp. $U_G^{(y)}$). We refer to $U_G^{(x)}$ and $U_G^{(y)}$ as the horizontal and vertical components of our virtual representation, and these determine the 1D portion of our SPTO signature. In particular, whether or not our system has nontrivial 1D SPTO is equivalent to whether or not the horizontal/vertical components of our representation are nontrivial projective representations of G. More concretely, the product of two elements of $U_G^{(\mu)}$, $U_g^{(\mu)}$ and $U_h^{(\mu)}$ (μ standing for either x or y), will generally only equal $U_{gh}^{(\mu)}$ up to a phase factor, such that $U_g^{(\mu)} U_h^{(\mu)} = \omega_2^{(\mu)}(g,h)\, U_{gh}^{(\mu)}$. Multiplication of elements of $U_G^{(\mu)}$ is associative, and this condition ends up forcing our phases $\omega_2^{(\mu)}(g,h)$ to be 2-cocycles. The cohomology classes of these horizontal and vertical cocycles, $[\omega_2^{(x)}]$ and $[\omega_2^{(y)}]$, then form the 1D components of Ω_2, the SPTO signature of $|\psi\rangle$.

Let's use these techniques to determine the SPTO signature of the 2D cluster state. We can choose a PEPS representation for a single qubit site of the 2D cluster state as $\mathcal{A}_C^{(1\times1)} = \sum_{i=0}^{1} |i\rangle \otimes A_i$, with the $A_i \in (H_v^*)^{\otimes 4}$ given by

$$A_0 = \langle +X, 0, +X, 0| \;\;,\;\; A_0 = \langle -X, 1, -X, 1|\,. \tag{C2}$$

H_v is here a qubit space, and the ordering of our systems in Eq. (C2) is as $(H_v^{(left)} \otimes H_v^{(right)} \otimes H_v^{(top)} \otimes H_v^{(bottom)})^*$. We are interested in the SPTO signature of the 2D cluster state with respect to a 2×2 unit cell, since the cluster state then has its maximal on-site symmetry group of $G = (\mathbb{Z}_2)^4$. To determine this, we contract together four copies of the PEPS tensor of Eq. (C2) to form a 2×2 PEPS tensor, $\mathcal{A}_C^{(2\times2)}$, and then find the virtual symmetry representations $U_G^{(x)}$ and $U_G^{(y)}$. These each act on a two-qubit virtual space, which for $U_G^{(x)}$ is decomposed as $(H_v^{(top)} \otimes H_v^{(bottom)})^*$, and for $U_G^{(y)}$ is decomposed as $(H_v^{(left)} \otimes H_v^{(right)})^*$.

As in the main text, we label the generators of $(\mathbb{Z}_2)^4$ by their respective locations in the 2×2 unit cell. One can then verify that the following choice of virtual symmetry representation makes our PEPS tensor $\mathcal{A}_C^{(2\times2)}$ an intertwiner with respect to the physical representation u_G (see Figure 6c):

$$\begin{aligned} U_{NW}^{(x)} &= Z \otimes I \quad U_{NW}^{(y)} = Z \otimes I \\ U_{NE}^{(x)} &= X \otimes I \quad U_{NE}^{(y)} = I \otimes Z \\ U_{SE}^{(x)} &= I \otimes X \quad U_{SE}^{(y)} = I \otimes X \\ U_{SW}^{(x)} &= I \otimes Z \quad U_{SW}^{(y)} = X \otimes I \end{aligned} \tag{C3}$$

The fact that we can choose a form for $\mathcal{U}_G$ which factorizes into parts and satisfies Eq. (C1) with $e^{i\theta_G} = 1$ is confirmation of the trivial 2D and 0D SPTO of the 2D cluster state. The only thing that remains is determining the two 1D components of the SPTO signature. We can show that these are both nontrivial by considering the commutation relation of elements of $U_G^{(x)}$ and $U_G^{(y)}$. While $(\mathbb{Z}_2)^4$ is abelian, the virtual representations in Eq. (C3) aren't, as shown by $U_{NW}^{(x)} U_{NE}^{(x)} (U_{NW}^{(x)})^\dagger (U_{NE}^{(x)})^\dagger = U_{NW}^{(y)} U_{SW}^{(y)} (U_{NW}^{(y)})^\dagger (U_{SW}^{(y)})^\dagger = -I^{\otimes 2}$. This means that the 2-cocycle $\omega_2^{(\mu)}$ associated with each of our virtual representations is different from the identity. Furthermore, multiplying either of these 2-cocycles by an arbitrary 2-coboundary is equivalent to modifying the phases associated to our individual $U_g^{(\mu)}$ as $U_g^{(\mu)} \mapsto \omega_1(g) U_g^{(\mu)}$, with $\omega_1(g) \in \mathcal{C}^1(G, U(1))$. This has no effect on the commutators of our symmetry group, which proves that our 2-cocycles $\omega_2^{(x)}$ and $\omega_2^{(y)}$ are in nontrivial 2-cohomology classes. The SPTO signature of the 2D cluster state is therefore $\Omega_2^{(C)} = \langle\langle\, 0\,;\, 1\,,1\,;\, 0\,\rangle\rangle$, meaning trivial 2D SPTO and nontrivial 1D SPTO, with the latter belonging to the nontrivial D_2 Haldane phase.

D. Proof of the Pauli Universality of Our Resource State

In this Section, we give a proof of the fact that our Union Jack resource state is Pauli universal, meaning that it can carry out universal MQC using only measurements of single-qubit Pauli operators. Achieving this universality requires several components, namely:

- We can convert regions of our Union Jack to "cluster regions", which are locally isomorphic to the 2D cluster state. This involves carrying out a pattern of computational basis measurements which converts (a part of) our state to a random graph state. The protocol of [6] (which uses only Pauli measurements) is then used to concentrate this state into a 2D cluster state, which in turn requires the percolation problem associated with our random graph states to lie in a supercritical phase. We demonstrate the supercriticality of this percolation problem, and thereby the ability to prepare cluster regions within our state, in Section D 1.

- We can teleport states and implement Clifford operations on them within the cluster regions of our state, using only Pauli measurements. Due to these cluster regions being identical to connected regions of the cluster state, we can use the same measurement patterns described in [8] to implement these Clifford operations, which use only Pauli measurements.

- We can create "interaction gadgets", which implement a three-qubit non-Clifford operation, $U_I^{(123)} = CCZ^{(123)} \sqrt{CZ}^{(12)} \sqrt{CZ}^{(23)}$, using only Pauli-basis measurements. Furthermore, these gadgets can be connected to a surrounding cluster region with a finite success probability, allowing us to use these gadgets as logical gates which we can connect together to create a CCZ operation. We demonstrate these various facts in Section D 2.

Taken together, these various facts successfully demonstrate the Pauli universality of our Union Jack state.

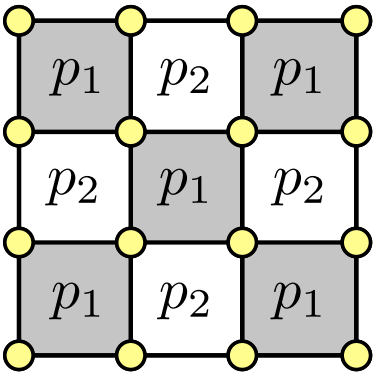

FIG. 7. A layout of our two-parameter percolation model. Cells labeled with p_i $(i = 1, 2)$ are independently sampled, such that the probability of obtaining an outcome of 1 in that cell is p_i. An edge of our random graph state is set when two adjacent nodes differ in their values. This yields a deterministically empty lattice at $(p_1, p_2) = (0, 0)$ or $(1, 1)$, and a deterministically full lattice at $(p_1, p_2) = (0, 1)$ or $(1, 0)$. Additionally, setting $p_1 = 0$ (resp. $p_2 = 0$) gives a percolation problem which is isomorphic to a site percolation problem on a square lattice with a bond probability of p_2 (p_1). Our problem of interest is located at $(p_1, p_2) = (\frac{1}{2}, \frac{1}{2})$.

1. Conversion to a 2D Cluster State

After giving a more complete description of the reduction of our $\mathbb{Z}_2$ resource state to a random graph state, we describe the simulations we use to verify that the associated percolation problem is indeed in the supercritical phase. These simulations involve the construction of a two-parameter model which includes as a special case the percolation problem associated to our random graph state reduction protocol. We show that our particular percolation problem lies within a supercritical phase, thus demonstrating that the protocol of [6] can be used

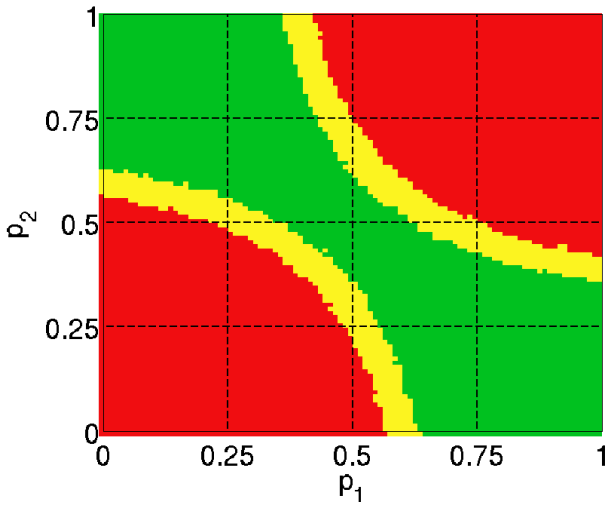

FIG. 8. The percolation phase diagram of our two-parameter model. Red (bottom left and upper right) indicates a subcritical phase, while green (upper left to bottom right) indicates a supercritical phase. The yellow region contains the critical line separating the phases. This division is based on the spanning probability p_{span} when $m = 100$, and in particular whether $p_{span} \leq 0.05$, $p_{span} \geq 0.95$, or $0.05 < p_{span} < 0.95$. From the placement of our problem of interest at $(p_1, p_2) = (1/2, 1/2)$, it is clear that we are within a supercritical phase, and can therefore use our 2D SPTO state as a universal resource for MQC.

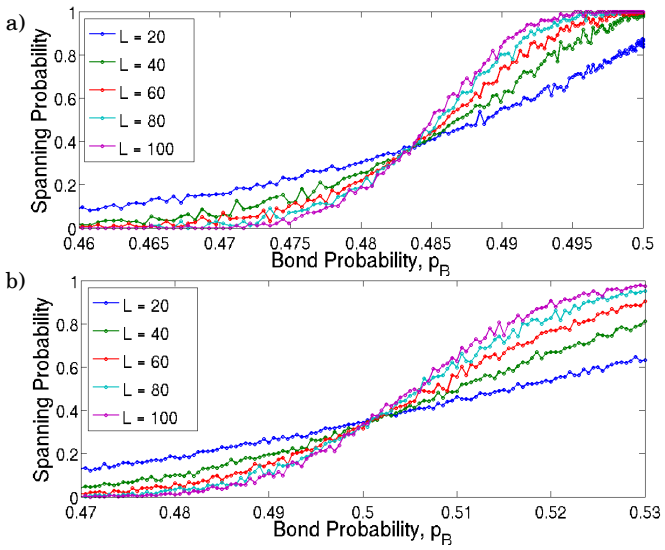

FIG. 9. a) The percolation probability for lattices of increasing linear size L, as we vary a parameter ϵ from 0 to 1. The marginal bond probability varies as $p_B = \epsilon(1 - \frac{1}{2}\epsilon)$, and the critical bond probability is seen to be $p_B = 0.484 \pm 0.001$. b) Using the same tools as were used in (a) to study the canonical square lattice bond percolation problem. The critical bond probability is known to be $\frac{1}{2}$, and our simulation reproduces this, locating it at $p_B = 0.500 \pm 0.001$.

to efficiently convert these random graph states to a 2D cluster state with arbitrarily high probability.

As described in the Methods, the method we use for reducing our 2D SPTO resource state to a random graph state consists simply of measuring all of the control sites in the computational basis. Given n control sites initially, upon measurement we obtain a string of random outcomes $\mathbf{c} = (c_1, c_2, \ldots, c_n)$. What is the reduced state of the logical portion of our system given a particular string of outcomes $\mathbf{c}$? To figure this out, we exploit the fact that the projector associated with our measurement outcome commutes with all of the CCZ's, since the latter are diagonal in the computational basis. Thus, the state of our system after measurement is the same as if we had initialized the control sites in their post-measurement states, and afterwards applied CCZ everywhere in our lattice. The resulting (unnormalized) state is then

$$\left|\tilde{\psi}(\mathbf{c})\right\rangle = \frac{1}{\sqrt{2^n}} \prod_{\ell \in \mathcal{L}_2} (CZ_\ell)^{c(\ell)+c'(\ell)} \left|+X\right\rangle^{\otimes n}. \qquad \text{(D1)}$$

Here, $\mathcal{L}_2$ is the collection of edges in our lattice, CZ_ℓ is a controlled-Z gate applied to the endpoints of a logical edge ℓ, while $c(\ell)$ and $c'(\ell)$ are the measurement outcomes obtained on the two control sites adjacent to ℓ. The factor of $1/\sqrt{2^n}$ emerges from the inner product of our n measurement outcomes $\langle 0|$ or $\langle 1|$ with the $|+X\rangle$'s which were used to initialize our state. What Eq. (D1) tells us (ignoring normalization) is that whenever the measurement outcomes on two adjacent control sites are not equal, a CZ operation is performed on the logical edge in between them, while nothing is done when the measurement outcomes are the same.

From this description, it is easy to see that every state $|\psi(\mathbf{c})\rangle$ is a graph state, whose edges lie only along domain walls of the control site measurement outcomes. The control site outcomes themselves are uncorrelated and uniformly distributed, which follows from the equal magnitude of all of the unnormalized reduced states in Eq. (D1). More precisely, the probability of obtaining a particular outcome $\mathbf{c}$, $p(\mathbf{c})$, is given by

$$p(\mathbf{c}) = \left\langle \tilde{\psi}(\mathbf{c}) \middle| \tilde{\psi}(\mathbf{c}) \right\rangle = \frac{1}{2^n}. \qquad \text{(D2)}$$

Ignoring the quantum origin of the probabilities, this probabilistic reduction to a graph state can be seen as defining a (classical) percolation problem, wherein edges of a graph are filled based on the configuration of random control site variables. We wish to conclusively determine whether this percolation problem, with site probabilities given by Eq. (D2), corresponds to subcritical or supercritical behavior in the large-system limit. More explicitly, from the known behavior of percolation problems, we expect that the probability of obtaining a connected graph component which connects arbitrarily distant portions of our lattice goes to either 0 or 1 as we make our system size larger, and we would like to know which of these possibilities holds.

To do this, we carry out numerical simulations of a two-parameter percolation model identical to ours, but with tunable probabilities for different control site outcomes. While Eq. (D2) corresponds to a probability of $\frac{1}{2}$ of obtaining 1 on any arbitrary control site, our variable model has probabilities of p_1 on one half of the sites, and p_2 on the other half of the sites. Figure 7 shows the checkerboard-style layout of these sites. The percolation problem defined by our actual system then corresponds to the point $p_1 = p_2 = 1/2$.

Figure 8 shows a phase diagram of this two-parameter model which demarcates the approximate locations of the subcritical and supercritical percolation phases. Although we haven't attempted to determine the exact location of the line of criticality which separates these two phases, it is clear that our system lies within the supercritical percolation phase.

Figure 9a shows the spanning probability we obtain along a one-parameter path through our configuration space. The path, parameterized by ϵ, travels along $p_1 = p_2 = \frac{1}{2}\epsilon$ for $0 \leq \epsilon \leq 1$. The marginal probability of obtaining a single bond in our lattice is $p_B = p_1 + p_2 - 2p_1p_2 = \epsilon(1 - \frac{1}{2}\epsilon)$ along our path. A percolation phase transition is seen to occur at $p_B = 0.484 \pm 0.001$. For comparison, in Figure 9b we show a simulation of the standard square lattice bond percolation problem, wherein bonds appear independently of each other with probability p_B. Using identical methods, we identify a phase transition at $p_B = 0.500 \pm 0.001$, in agreement with the known exact value of $p_B = \frac{1}{2}$.

These results, along with the percolation results in Figure 4, conclusively demonstrate the supercritical behavior of the random graph states obtained in our state reduction protocol, thus proving our ability to prepare cluster regions within our Union Jack state using only Pauli basis measurements.

2. Non-Clifford Gates using our Interaction Gadget

We first prove that our interaction gadget, associated with the measurement pattern shown in Figure 10a, implements the unitary gate $U_I^{(123)} = CCZ^{(123)}\sqrt{CZ}^{(12)}\sqrt{CZ}^{(23)}$, and we give the Clifford byproduct operators associated with certain unintended measurement outcomes. We then discuss how such gadgets can be embedded into a surrounding cluster region, allowing them to act on arbitrary triples of qubits within that region.

The core of our interaction gadget is the three-body operation given by multiplying two overlapping copies of CCZ and contracting one of the overlapping sites with an ancilla state $|+X\rangle$ and a Y-basis measurement outcome $\langle \pm Y| = \frac{1}{\sqrt{2}}(\langle 0| \mp i \langle 1|)$. Choosing $\langle +Y|$ to be the ideal outcome, this yields the operation

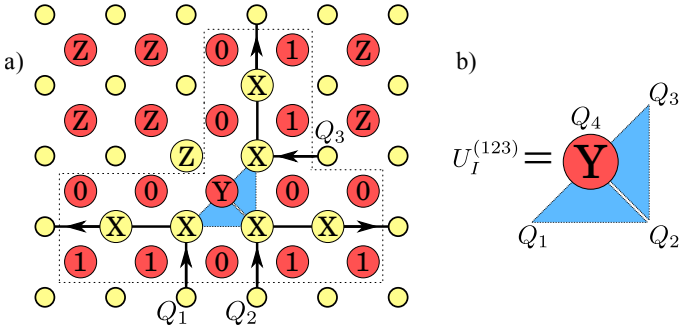

FIG. 10. a) Our interaction gadget, which allows us to apply the gate U_I to logical information. Blue triangles here represent CCZ gates involved in forming the Union Jack state which play nontrivial roles in preparing U_I. We measure one control site in the Y-basis, six logical sites in the X-basis, and one logical site (along with many surrounding control sites) in the Z-basis, then use postselection to fix 13 of the control site measurement outcomes. The postselection is necessary to guarantee we can teleport information through the interaction gadget, the teleportation being carried out with the six X-basis measurements. b) The three-body operation which produces the diagonal unitary gate, U_I. Qubit 4 is initialized in a $|+X\rangle$ state, then contracted with a $\langle +Y|$ outcome.

$$U_I^{(123)} = \langle +Y|^{(4)} \left(CCZ^{(124)} CCZ^{(234)} \right) |+X\rangle^{(4)}, \quad \text{(D3)}$$

which is diagonal in the computational basis (shown in Figure 10b). Up to overall normalization and phase, $U_I^{(123)}$ gives a phase factor of i when acting on $|110\rangle^{(123)}$ or $|011\rangle^{(123)}$, and a phase factor of 1 otherwise, proving that its operation is identical to $CCZ^{(123)}\sqrt{CZ}^{(12)}\sqrt{CZ}^{(23)}$. Because $\langle -Y| = (\langle +Y|)^*$, the operation given by the outcome $\langle -Y|$ is $(U_I^{(123)})^*$, which is equal to $U_I^{(123)}$ up to Clifford byproduct operators $CZ^{(12)}CZ^{(23)}$.

The three-body operation discussed above assumes that a $\langle 0|$ outcome has been obtained in the logical site Z measurement adjoining the control site Y measurement (yellow Z in Figure 10a), and thus needs to be modified when a $\langle 1|$ outcome is obtained. In this latter case, the overlapping $CCZ^{(124)}CCZ^{(234)}$ in Eq. (D3) is replaced by $CCZ^{(124)}CCZ^{(234)}CZ^{(14)}CZ^{(34)}$, and it can be shown that the resultant gate is again equal to $U_I^{(123)}$ up to Clifford byproduct operators $S^{(1)}S^{(3)}$, where S is the phase gate $S = \mathrm{diag}(1, i)$. Finally, the case of unintended Y and Z outcomes in conjunction leads to Clifford byproduct operators $(CZ^{(12)}CZ^{(23)}S^{(1)}S^{(3)})^\dagger$.

In summary, we have shown that a combined Y and Z measurement is capable of converting two non-Clifford CCZ gates into a three-body non-Clifford U_I gate, with variation in measurement outcomes being accounted for by Clifford byproduct operators. Now how do we use this three-body unitary as a logical operation? One method

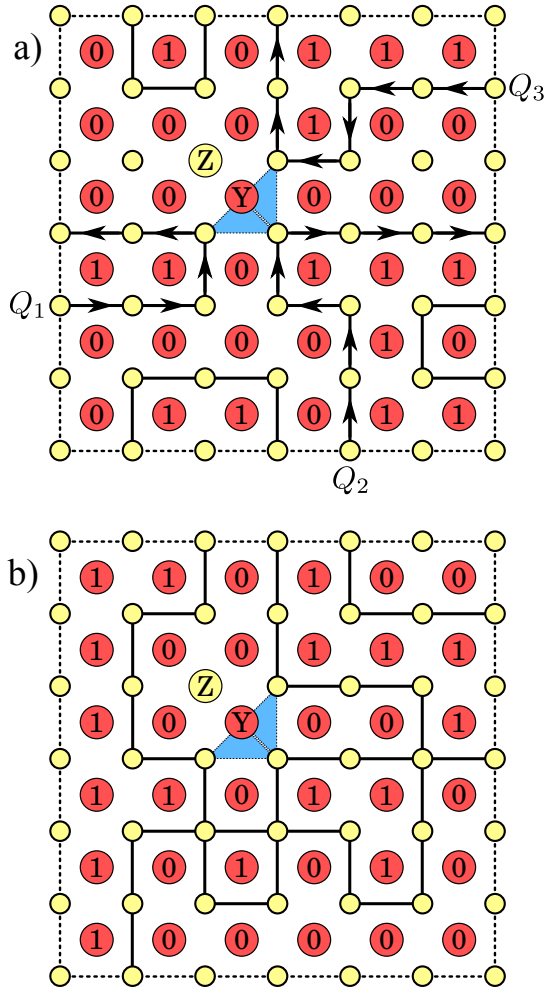

FIG. 11. a) A pattern of control site outcomes which possesses the "correct wiring" for our interaction gadget (X-basis measurements not shown). The wires percolate towards separate points on the boundary without intersecting each other and without being acted on by stray CZ gates. b) An incorrect wiring pattern, which would require us to try again somewhere else in order to obtain a usable interaction gadget. Note that such regions can still be used as portions of cluster regions, without impacting the overall efficiency of our protocol. In this case the control site marked Y would instead be measured in the computational basis.

for doing this is by measuring the control sites surrounding our interaction gadget in the computational basis, and then attempting to use the random graph state we obtain to teleport qubits through the sites which U_I acts on. In the process of teleporting this information, U_I is successfully applied to the three qubits of interest. However, we aren't guaranteed to obtain a graph state with the "correct wiring", i.e. one for which we can separately teleport each logical qubit to and from its respective site adjoining the interaction gadget, as in Figure 11a. Because of the possibility of obtaining graph states with incorrect wiring patterns, the successful embedding of an interaction gadget into a surrounding cluster region only occurs with some probability, which generically depends on the size of the surrounding cluster region.

We can show that the probability of obtaining a correct wiring pattern in the large system limit is finite and non-zero, by exploiting the same supercritical percolation properties which allowed us to prove the successful preparation cluster regions. This constant success probability then guarantees that the stochastic nature of our interaction gadget embedding only contributes a constant multiplicative factor to the number of sites measured in our protocol. Consequently, our MQC protocol gives a proof of principle demonstration that we can efficiently perform quantum computation. Our proof involves first restricting ourselves to a region of finite size surrounding a particular interaction gadget, then using postselection (with finite success probability) to obtain a pattern of control qubit measurement outcomes which prepares a graph state with the correct wiring. For example, choosing a 6×6 grid of control qubits, we could postselect for the pattern shown in Figure 11a.

When our region is of sufficient size, our postselected pattern can always be chosen so that distinct logical wires percolate without intersecting each other, and end at sufficiently separated points on the boundary of this region. When the separation between adjacent wire endpoints on the boundary of our finite region is much greater than the characteristic percolation length scale (the length scale associated with the exponential decay seen in Figure 4), the conditional probability of continuing our postselected pattern to a macroscopic graph state with the correct wiring factorizes into six uncorrelated probabilities. These probabilities, one for each wire, encode the chance of each wire percolating to a point infinitely far from its starting point on the finite region boundary. Because of the supercritical nature of this percolation, each of these conditional success probabilities is finite, meaning that the total success probability for embedding an interaction gadget in a large cluster region is finite. Thus, our interaction gadgets can be embedded in cluster regions with a constant multiplicative overhead, letting us efficiently use them as logical gates which, together with the Clifford gates we get from our cluster regions, form a universal gate set.

[1] X. Chen, Z.-C. Gu, Z.-X. Liu, and X.-G. Wen, *Symmetry Protected Topological Orders and the Group Cohomology of Their Symmetry Group*, Phys. Rev. B **87**, 155114 (2013).

[2] M.P. Zaletel, *Detecting Two-Dimensional Symmetry-Protected Topological Order in a Ground-State Wave Function*, Phys. Rev. B **90**, 235113 (2014).

[3] D.J. Williamson, N. Bultinck, M. Mariën, M.B. Sahinoglu,

J. Haegeman, and F. Verstraete, *Matrix Product Operators for Symmetry-Protected Topological Phases*, arXiv:1412.5604, (2014).

[4] X. Chen, Z.-X. Liu, and X.-G. Wen, *Two-Dimensional Symmetry-Protected Topological Orders and Their Protected Gapless Edge Excitations*, Phys. Rev. B **84**, 235141 (2011).

[5] M. Levin and Z.-C. Gu, *Braiding Statistics Approach to Symmetry-Protected Topological Phases*, Phys. Rev. B **86**, 115109 (2012).

[6] D.E. Browne, M.B. Elliott, S.T. Flammia, S.T. Merkel, A. Miyake, and A.J. Short, *Phase Transition of Computational Power in the Resource States for One-way Quantum Computation*, New J. Phys. **10**, 023010 (2008).

[7] R. Raussendorf and H.J. Briegel, *A One-Way Quantum Computer*, Phys. Rev. Lett. **86**, 5188 (2001).

[8] R. Raussendorf, D.E. Browne, and H.J. Briegel, *Measurement-Based Quantum Computation on Cluster States*, Phys. Rev. A **68**, 022312 (2003).